UDC 621.9.048.7

PHYSICAL AND MECHANICAL PROPERTIES OF TITANIUM ALLOY VT1-0 AFTER HIGH-CURRENT ELECTRON BEAM IRRADIATION

V.F. Klepikov[1], Yu.F. Lonin[2], A.G. Ponomarev[2], O.A. Startsev[1], V.T. Uvarov[2]
[1]Institute of Electrophysics and Radiation Technologies NAS of Ukraine, Kharkov, Ukraine
E-mail: startsev-alex@ukr.net;
[2]NSC "Kharkov Institute of Physics and Technology", Kharkov, Ukraine

Titanium alloy VT1-0 was modified by the high-current electron beam irradiation with energy 0.35 MeV, 5 μs impulse, and power density of 60 MW·cm^{-2}. It was found that intense electron exposure significantly increased both hardness (by 30%) and elastic modulus (by 12%) within a subsurface layer of 100 μm thick. The thermoelastic model of the metal ablation was developed. Description of dynamics of the induced temperature and deformations distributions has been performed using the finite difference and finite element methods.

INTRODUCTION

The purpose of present work is to investigate the dynamics of the modification processes in the ultrafine grained α-Ti-alloy VT1-0 under the exposure of the microsecond HCEB [1, 2]. This topic is considered with particular attention to formation of new structures in the material volume after modification. We concentrate our efforts on simulation of the relevant conditions under irradiation. These studies are claimed to reveal (i) the induced changes in microstructure, hardness and elastic modulus values, (ii) the heating and cooling temperature rates and their gradients, along with (iii) the thermal displacements and residual stresses.

1. MATERIALS AND METHODS

A plate of Ti-alloy VT1-0 (Ti > 99.2 wt.%) [3] was irradiated in vacuum by one impulse at the TEMP-A pulsed e-beam accelerator facility with the current of 2 kA, electron energy of 0.35 MeV, impulse duration $\tau_p \sim 5$ μs, and the average heat flux factor of around 1.3 GW·s$^{1/2}$·m^{-2}. The thickness of the plate was 2 mm. The Gaussian-shaped hollow cross-sectional beam had the inner and outer radii of 20 and 28 mm, respectively. The beam's full-width half-maximum was around of 2 mm. Visual and morphological analysis of the irradiated plate and its cross-fractures was performed by the light microscope Bresser BioLux NV. Fractographic analyses of the cross-fractures were conducted using the scanning electron microscope JEOL JSM-840. The hardness H_{50} properties were measured by the PMT-3 microhardness testing machine Estimates of the elastic modulus E and nanohardness H were obtained using the Nano Indenter G200. Numerical simulations of temperature and deformations dynamics were conducted using finite difference (FD) and finite element (FE) methods. The numerical scheme was adopted in terms of weak formulation and implemented in FreeFem++ [4].

2. THERMOELASTIC MODEL OF E-BEAM ABLATION

We will evaluate the induced temperature field and displacements inside the bulk solving a corresponding two-dimensional thermo-mechanical problem in $\{x,y\}$ spatial coordinate system. A model specimen is a homogeneous plate $\{0..H_x \times 0..H_y\}$ in $\Omega \in R^2$, when its width is greater than a thickness $H_y > H_x$. A plate is subjected to the irradiation perpendicular to its front surface $\Gamma_1 = \{0 \times 0..H_y\}$, otherwise Γ_2 is the nonirradiated surface. The hyperbolic equation for heat conduction, based on Maxwell – Cattaneo – Lykov law is (1):

$$\frac{\partial T}{\partial t} + \tau_r \frac{\partial^2 T}{\partial t^2} = \frac{1}{\rho c}\{\nabla \cdot (k \nabla T(\vec{r},t)) + \\ + \tau_r \nabla \cdot (k \nabla \frac{\partial T}{\partial t}) + Q + \tau_r \frac{\partial Q}{\partial t}\}, \quad (1)$$

where c is the thermal capacity; ρ – the material density; k – the coefficient of thermal conductivity; τ_r is the electron-phonon relaxation time, and the heat source power function Q. Initially, the sample is at uniform temperature T_0. The boundary conditions are:

$$T(\vec{r},t)\big|_{\Gamma_2} = T_0, \quad (2)$$

$$k \frac{\partial T(\vec{r},t)}{\partial r}\bigg|_{\Gamma_1} + m^2 \sigma_R \varepsilon_R (T^4 - T_0^4) = Q_e(\vec{r},t)\big|_{\Gamma_1}, \quad (3)$$

where ε_R is the integral emissivity; σ_R is Stefan's constant, and m – the refractive index of the environment, and the right part denotes the absorbed heat flux per unit area. The equation of equilibrium is (4), where we introduce the body force f caused by the thermal expansion (5), and use Hooke's law in the following constitutive relation (6):

$$\nabla \cdot \sigma_{ij}(u,T) + f_i = 0, \quad (4)$$

$$f_i = \nabla \cdot ((3\lambda + 2\mu)\alpha_T (T - T_0)\delta_{ij}), \quad (5)$$

$$\sigma_{ij}(u,T) = 2\mu\varepsilon_{ij} + \delta_{ij}\lambda\varepsilon_{ii}, \quad (6)$$

$$\varepsilon_{ij}(u) = \frac{1}{2}(\frac{\partial u_i}{\partial x_j} + \frac{\partial u_j}{\partial x_i}), \quad (7)$$

where σ is the stress tensor; ε is the small strain tensor (7); $\vec{u}$ is the displacement vector; λ, μ are the isothermal Lame's coefficients; α_T is the linear coefficient of thermal expansion. The boundary conditions for the elastic part are (8), (9), where g is a surface force by the expanding plasma torch, $\vec{n}$ is the normal unit vector, η_{ef} is the ratio of the thermal capacities of solid medium to generated plasma, ω_{loc} is the local volumetric energy absorption density.

$$\sigma_{ij} n_j\big|_{\Gamma_1} = g_i = -n_i \omega_{loc}(\eta_{ef} - 1), \quad (8)$$

$$u\big|_{\Gamma_2} = 0. \quad (9)$$

Let us define the heat source power function Q (10) as a sum of energy released by the e-beam in a solid Q_e, and a correlation additive Q_σ related to take into account the impact of deformation on the temperature distribution [5]. We can denote Q_e in (11) by the current density $j(\vec{r},t)$ (12) over the total irradiated surface area S_{irr}, the linear energy loss of electrons in a solid $\partial E / \partial x$.

$$Q = Q_e + Q_\sigma, \quad (10)$$

$$Q(\vec{r},t) = j(\vec{r},t) \cdot \frac{\partial E}{\partial x}, \quad (11)$$

$$j(\vec{r},t) = \frac{J}{S_{irr}} \prod_{i=y,t} \frac{1}{\sqrt{2\pi d_\xi^2}} e^{\frac{-(\xi-\xi_i)^2}{2d_i^2}}. \quad (12)$$

The heat expansion influences on the temperature field and on overall ablation picture significantly. Q_σ denotes how temperature changes in response of sample's deformation (13). The energy absorption density ω_{loc} of a local volume dV during some exposure time is given by (14), where ϵ is the absorption coefficient, that can be calculated in CASINO.

$$Q_\sigma = -(3\lambda + 2\mu)\alpha_T T_0 \dot{\varepsilon}_{ii}, \quad (13)$$

$$\omega_{loc} = \epsilon \int_0^t \int_{dV} Q_e(\vec{r},t)dtdV \Big/ \int_{dV} dV. \quad (14)$$

3. FINITE DIFFERENCE AND FINITE ELEMENT MODELLING

Thereunder, we use FD method to discretize the time operators by replacing a time differential with an approximate expression using the differential formulas. Applying FE approach, discretize an underlying space domain. Such a combination of FE and FD methods helps to avoid the spatial oscillations of solutions and considering the time evolution in FreeFEM. Then, we reformulate the system (1)–(14) into the weak form, which requires the unknown functions be continuously differentiable until first partial derivative. For time discretization we apply the forward difference scheme. A general adaptation scheme (15) is used for designation of spatial variables in (1), (4)–(7), when θ denotes the type of scheme (if $\theta = 1/2$ – Crank-Nicolson scheme, etc).

$$\varsigma^{i+\theta} = \theta\varsigma^{i+1} + (1-\theta)\varsigma^i, \text{ where } \varsigma = \{T, u\}. \quad (15)$$

The temperature equation (1) multiplied by the weight function υ and written in the variational form is (16). The elasticity part of problem (4)–(7) is rewritten with the supplementary weight function w (17).

$$\begin{aligned} &T^{i+1}(\tau+\tau_r) - T^i(\tau+2\tau_r) + \tau_r T^{i-1} = \\ &= \frac{\tau^2}{\rho c}\Big[\int_\Omega k\{\nabla T^{i+\theta}\cdot\nabla\upsilon - \tau_r\chi^i\nabla T^{i+1}\cdot\nabla\upsilon\}d\Omega + \\ &+ \int_\Omega \{Q^{i+\theta}(1-\frac{\tau_r}{\tau}) + Q^{i+1+\theta}\frac{\tau_r}{\tau}\}\upsilon d\Omega\Big], \\ &\text{where } \chi^i\tau = 1 - T^i / T^{i+1}, \end{aligned} \quad (16)$$

$$\begin{aligned} &\int_\Omega \{2\mu\varepsilon_{ij}(u^{i+\theta})\varepsilon_{ij}(w) + \lambda\varepsilon_{ii}(u^{i+\theta})\varepsilon_{jj}(w)\}d\Omega - \\ &-\int_\Omega \{(3\lambda+2\mu)\alpha_T\nabla T\cdot w\}d\Omega + \\ &+\int_{\Gamma_1} \{\omega_{loc}(\eta_{eff}-1)w\}d\Gamma = 0. \end{aligned} \quad (17)$$

However, we cannot find the values of Q^{i+1} and Q^{i+2}, while Q is not deterministic in our case, as $\partial E / \partial x$ and $\dot{\varepsilon}_{ii}$ are unknown in "future" without solving step-by-step (16)–(17). Thus, we can operate only with the previously obtained values of Q^i, Q^{i-1} (e.g. backward Euler scheme). Hence, these restrictions result in truncated over θ discretization scheme. Finally, we separate the bilinear form and the linear form in (16)–(17), add the Dirichlet boundary conditions (2), (9) by embedded operator 'on', include subroutine for iterative solving of radiative condition (3) [3], than apply the classical continuous Galerkin method to solve the final system in FreeFEM using a finite basis of the quadratic P_2 Lagrangian elements.

The material parameters of VT1-0 used in the calculations are: c = 540 J·kg^{-1}·K^{-1}; ρ = 4505 kg·m^{-3}; k = 18.85 W·m^{-1}·K^{-1}; Young's modulus E = 117 GPa; Poisson's ratio ν = 0.32; α_T = 8.2·10^{-6} K^{-1}; η_{eff} = 1.2; ϵ = 0.87; τ_p = 5·10^{-6} s; τ_r = 10^{-12} s; m = 1; ε_R = 0.5; σ_R = 5.67·10^{-8} W·m^{-2}·K^{-4}; H_x = 5·10^{-4} m; H_y = 2·10^{-3} m, and J = 2·10^3 A; U = 0.35·10^6 V; ξ_y = 5·10^{-3} m; ξ_t = 2.5· 10^{-6} s; d_y = 2.1·10^{-3} m; d_t = 1.06·10^{-6} s.

4. RESULTS AND DISCUSSION

The HCEB irradiation of the Ti-alloy VT1-0 provoked fast inhomogeneous heating, significant volumetric damage to the sample, formation of crater and multilayered subsurface structure. Among the damage mechanisms of VT1-0 we distinguished melting (liquid ejection), evaporation, and thermal stresses. The melting mechanism was predominant because the remaining melt has not been totally removed from the crater during the impulse duration. Almost 2/3 of the melt was resolidified in the track's hollow and the amount of evaporated metal was very low. The melt, ejected during hydrodynamic sputtering, was condensed on the periphery surface as the nonuniform droplet cover with the droplet size of 2…30 μm. The maximum crater depth is $h \sim$ 0.5 mm, which is around of two maximum characteristic pass lengths of 0.35 MeV electrons R = 0.23 mm. The surface of track is very rough and wavy with the average roughness ~ 0.15 mm.

The development of fracture processes in the irradiated Ti-alloy VT1-0 is quite different to features occurring in the nonirradiated metal (Fig. 1). Fractographic data permit to distinguish several zones with the different microstructure: quenching zone (see QZ, Fig. 1 mark A), heat (e.g. melting) and shock-wave-affected zone (see HAZ, Fig. 1 mark B). Nonirradiated material is characterized by the rough fracture surface of α-phase with a ductile fracture mechanism with equiaxed globular grains with linear size up to 10 μm. The microstructure of the 'as-fabricated' metal has not any preferred orientation.

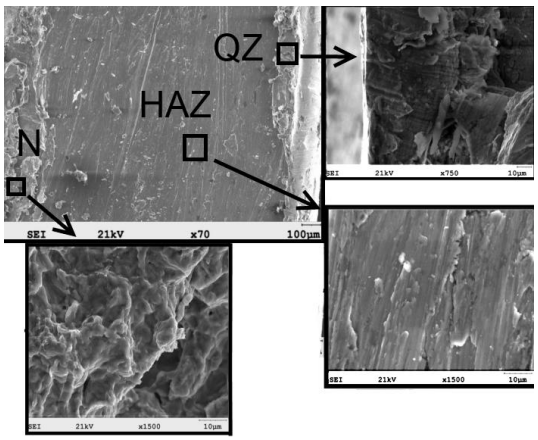

Fig. 1. Microstructure of cross-sectional breaks of VT1-0 Titanium alloy, where (QZ) – quenched zone, (HAZ) – heat-and shock-wave-affected zone and (N) is 'as-fabricated' nonirradiated alloy

The thickness of QZ varying in interval 50…150 μm with the maximal value in the epicenter of exposure. The HAZ zone is around of 1 mm thick in the epicenter and 200 μm in the periphery. Both QZ and HAZ are characterized by the brittle fracture mechanism and the same average linear grain size of approximately 100 μm. QZ was formed during rapid cooling of the residual melt and the back condensed gas-droplet cloud. The growth of temperature gradients resulted in increasing of thermomechanical stresses, giving rise to the accumulation of structural defects and high compressive stresses at the surface, which led to surface cracking. In grains' substructure of the QZ, we clearly distinguished the density lines almost normal to the surface. The thickness of one layer is less than 1 μm. HAZ has a highly compacted nonporous lamellar structure of elongated grains parallel to the surface, with negligible amount of intergrain fractures. This zone has relatively flat fracture surface compared to the nonirradiated part. The well-defined layers of different density were noticed all over the heterogeneous lamellar microstructure. These dense packed layers demonstrate the transgrain character through all HAZ. They have preferred orientation parallel to the surface. Such behavior of HAZ could be induced by the thermal fixation of the compactified melt during shock-wave impact. The thickness of density lines in HAZ is the same as in QZ. This zone was created during surface cracking of the upper border of HAZ upon the accumulated compressive surface stresses. However, it is not clear, how the cracked grains formed relatively smooth (in microscopic sense) surface with no trace of any big voids. As a result of microstructure modification, the mechanical properties have been altered significantly (Table). We measured micro- and nanohardness in the same regions for the nonirradiated, QZ and HAZ. We found, the microhardness and elastic modulus in the QZ were increased by 30 and 12%, respectively, in comparison with the initial parameters. The average microhardness in the HAZ is less by 10%, otherwise the Young's modulus is higher by 6%, comparatively. An increase of the Young's modulus and relative softening in the HAZ are attributed to formation of the lamellar martensite microstructure, which correspond with results in [2]. The efficient hardening of VT1-0 in the QZ might be induced during fast cooling by refinement and compactification of martensite under high tensions and residual heat supply form the bulk. Simulation of the temperature field (Fig. 2) and displacements (Fig. 3) in the realistic plate under HCEB exposure was conducted using the stated thermoelastic model with the constant time step of $1 \cdot 10^{-7}$ s, on the nonuniform mesh (824957 triangles, 414330 vertices) adapted to the energy deposition profile, and $\theta = 0.5$. The ablative mode provides extreme heating rates of (10^6…10^8) K/s in the epicenter of irradiation, and (10^4…10^6) K/s in the periphery regions. High temperature gradients up to 10^7 K/m are generated in the 1 mm surface layer. After the end of irradiation, radiative heat transfer and heat conductance into the bulk of metal induce high cooling rates and gradients of 10^7 K/s and 10^8 K/m in QZ, 10^2…10^4 K/s and 10^4 K/m in HAZ.

Hardness results and elastic modulus of 'as-fabricated' and irradiated VT1-0

VT1-0 Ti-alloy	Micro-hardness H_{50}, GPa	Nano-hardness H, GPa	Elastic Modulus E, GPa
Nonirradiated	2.3	2.8	117
Quenched zone	3.5	3.6	132
Heat- and hock-wave-affected zone	2.1	2.7	124

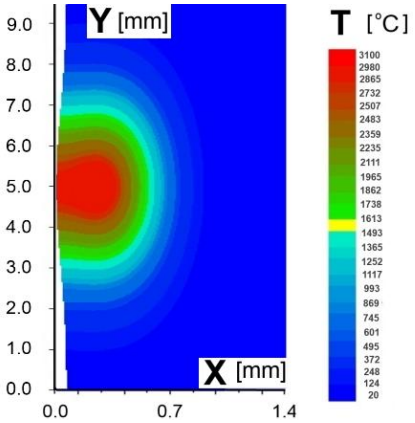

Fig. 2. Temperature distribution in titanium at the end of HCEB exposure

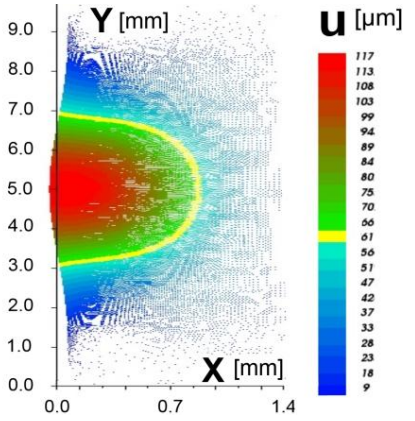

Fig. 3. Displacements in titanium at the end of HCEB exposure

The maximal deformations (see Fig. 3) of 100..120 μm achieved during fast heating in the epicenter, but finally disappeared due to further melting and annealing throughout the solidification. We can estimate the residual compressive stresses at the surface after irradiation. If we neglect the relaxation processes during cooling, the residual stresses would have the approximate values of 450 MPA. If we include into calculations the thermal relaxation of residual stresses, their estimated values would be around 150 MPA.

However, there are serious restrictions on predictions: one should be careful with inherited errors along with mesh adaptation upon the energy deposition profile, because it could generate numerical instabilities and disposed to oscillation remeshing artifacts. Additionally, to describe more accurately the phase transitions during the modification process it is necessary include into consideration the hydrodynamic description with free boundaries. This will help to simulate properly the melt dynamics and related mass transfers for formation of a crater and complex subsurface structure in the processed volume.

CONCLUSIONS

The HCEB irradiation of the Ti-alloy VT1-0 in ablative mode hardened the 100 μm surface layer by 30% compared to the nonirradiated material. Young's modulus increased by 12%. It caused embrittlement in the quenched and melted zones up to the depth of 1 mm. The model of thermal response of metals to the intense e-beam heating in microsecond timescale was developed and solved numerically using the FD time discretization and the FE approximation in terms of the classical Galerkin method. The calculated temperature fields, displacement distributions and residual stresses envisage the extreme conditions of the HCEB impact.

REFERENCES

1. A.B. Batracov et al. The particularities of the high current relativistic electron beams influence on construction materials targets // *Problems of Atomic Science and Technology. Ser. "Nucl. Phys. Inv."* 2013, N 6, p. 225-229.

2. V.T. Uvarov et al. Radiation acoustic control over the thermal parameter of construction materials irradiated by intense relativistic electron beam // *Phys. of Part. and Nucl. Latter*. 2014, v. 11, N 3, p. 274-281.

3. A.N. Dovbnya et al. Investigation of the surface of KhVG, Kh10N10T steels and VT-1 Titanium after irradiation with electron beam of the accelerator based on the magnetron gun with a secondary-emission cathode // *Problems of Atomic Science and Technology.* 2009, N 6, p. 134-140.

4. F. Hecht. New development in FreeFem++ // *J. Numer. Math*. 2012, v. 20, N 3-4, p. 251-265, 65Y15.

5. E.M. Kartashov, L.M. Ozherelkova. The new model ideas in the problem of thermal shock // *Matematicheskoe Modelirovanie*. 2002, v. 14(2), p. 95-108 (in Russian).

Статья поступила в редакцию 06.02.2015 г.

ФИЗИКО-МЕХАНИЧЕСКИЕ СВОЙСТВА ТИТАНОВОГО СПЛАВА ВТ1-0 ПОСЛЕ ОБЛУЧЕНИЯ СИЛЬНОТОЧНЫМ ЭЛЕКТРОННЫМ ПУЧКОМ

В.Ф. Клепиков, Ю.Ф. Лонин, А.Г. Пономарев, А.А. Старцев, В.Т. Уваров

Титановый сплав ВТ1-0 модифицирован сильноточным электронным пучком с энергией 0,35 МэВ, импульсом 5 мкс и плотностью мощности 60 МВт·см$^{-2}$. Обнаружено, что облучение интенсивным электронным пучком существенно увеличивает твердость (на 30%) и модуль упругости (на 12%) приповерхностного слоя толщиной 100 мкм. Построена термоэластическая модель абляции металла, согласно которой проведено описание динамики распределений температуры и деформаций методами конечных разностей и конечных элементов.

ФІЗИКО-МЕХАНІЧНІ ВЛАСТИВОСТІ ТИТАНОВОГО СПЛАВУ ВТ1-0 ПІСЛЯ ОПРОМІНЕННЯ СИЛЬНОСТРУМОВИМ ЕЛЕКТРОННИМ ПУЧКОМ

В.Ф. Клепіков, Ю.Ф. Лонін, А.Г. Пономарьов, О.А. Старцев, В.Т. Уваров

Титановий сплав ВТ1-0 модифіковано сильнострумовим електронним пучком з енергією 0,35 МеВ, імпульсом 5 мкс і густиною потужності 60 МВт·см$^{-2}$. Виявлено, що опромінення інтенсивним електронним пучком суттєво збільшує твердість (на 30%) та модуль пластичності (на 12%) приповерхневого шару товщиною 100 мкм. Розвинено термоеластичну модель абляції металу, згідно з якою здійснено опис динаміки розподілів температури та деформацій методами скінченних різниць та скінченних елементів.